Determination of D_s^+ meson fragmentation functions through two different approaches

Maral Salajegheh,[1,*] S. Mohammad Moosavi Nejad,[1,2,†] and Mahdi Delpasand[1,‡]
[1]*Faculty of Physics, Yazd University, P.O. Box 89195-741, Yazd, Iran*
[2]*School of Particles and Accelerators, Institute for Research in Fundamental Sciences (IPM), P.O. Box 19395-5531, Tehran, Iran*

(Received 4 September 2019; published 20 December 2019)

The hadronization mechanism is described by the fragmentation functions (FFs) which are universal and process-independent quantities. They can be generally determined theoretically or phenomenologically. In the phenomenological approach which is based on the data analysis, we present the FFs of D_s^+ both at leading-order (LO) and next-to-leading order (NLO) and, for the first time, at next-to-next-to-leading order in the minimal subtraction factorization scheme with five massless quarks. These functions are determined by fitting all available experimental data of inclusive single D_s^+-meson production in electron-positron annihilation, from the OPAL Collaboration at CERN LEP1. We shall also estimate the uncertainties in these FFs as well as in the corresponding observables. In the theoretical approach, we apply the perturbative FFs formalism based on the Suzuki's model and present our analytical results at LO and NLO perturbative QCD framework. For the first time, a comparison between both approaches will be presented in this work. We also apply our new FFs to generate theoretical predictions for the energy distribution of D_s^+ mesons produced through the decay of unpolarized top quarks, to be measured at the CERN LHC.

DOI: 10.1103/PhysRevD.100.114031

I. INTRODUCTION

For a long time, there has been considerable interest in the study of production mechanism of charmed-flavored hadrons (D-hadrons) at hadron and electron-positron colliders, both experimentally and theoretically. The study of properties of these heavy mesons provides us a possibility for better understanding the quark-gluon interaction dynamics in the QCD framework. Presently, there is particular interest in hadron production at the CERN Large Hadron Collider (LHC) and the BNL Relativistic Heavy Ion Collider due to ongoing experiments.

In general, two various mechanisms are assumed for the production of heavy hadrons: recombination and fragmentation. In the recombination scheme, as an example, heavy mesons are formed through the combination of heavy-light or heavy-heavy quarks which are produced independently in hard subprocesses. At sufficiently large transverse momentum of heavy hadron production, the recombination mechanism (or direct production scheme) is normally suppressed while the fragmentation one becomes dominant [1]. Fragmentation refers to the process of a parton which carries large transverse momentum and subsequently decays to form a jet containing the expected colorless hadron [2]. Therefore, fragmentation functions (FFs) describing the hadronization processes, along with the parton distribution functions (PDFs) of initial hadrons (in hadron-hadron or lepton-hadron collisions), are needed as nonperturbative inputs for the calculation of hadron production cross sections. Specifically, their specific importance is for their model-independent predictions of the cross sections. The universality feature of FFs allows one to transfer experimental information from, for example, electron-positron annihilation to any other production mechanism, such as photoproduction, leptoproduction, hadroproduction, and two-photon scattering.

Due to the importance mentioned for the FFs, of interest is to accurate determination of FFs as much as possible. Generally, two various approaches are used for determination of the nonperturbative FFs, which are known as the theoretical and phenomenological approaches. Independent of the approach used, when FFs are calculated at the initial scale of fragmentation one can evolve them to higher scales using the timelike Dokshitzer-Gribov-Lipatov-Altarelli-Parisi (DGLAP) renormalization group equations [3]. In the phenomenological approaches which are frequently used to determine the nonperturbative FFs, all free parameters in the proposed forms of the FFs are extracted form experimental data analysis; see, e.g., Refs. [4–7] and references therein. In this approach, FFs are calculated with high accuracy up to second-order approximation in QCD [8–15]. In an alternative approach which is based on

*M.Salajegheh@stu.yazd.ac.ir
†mmoosavi@yazd.ac.ir
‡Delpasand.mahdi@yahoo.com

the theoretical models, one can compute the heavy quark FFs by virtue of perturbative QCD with limited phenomenological parameters [16,17]. In Refs. [18–25], using the Suzuki's model [26], the FFs of heavy hadrons are calculated using the convenient Feynman diagrams at each order of perturbative QCD for the parton level of the process. Of its advantage is to include the spin information of hadrons into the corresponding FFs as well as the bound state nonperturbative dynamics of produced hadrons through the wave functions of bound states [27].

In this paper, we first apply the theoretical approach to compute the initial scale FF of charm quark to split into the S-wave D_s^+ meson at leading-order (LO) as well as next-to-leading order (NLO) perturbative QCD. In the following, using the phenomenological approach, a comprehensive QCD analysis is performed to obtain a set of gluon-, charm-, and bottom-quark FFs into the D_s^+ meson through a global QCD fit to the electron-positron single inclusive annihilation (SIA) data measured by OPAL Collaboration [28,29] at the CERN LEP1 collider. In Ref. [30], the nonperturbative D_s^+-FFs were determined both at LO and NLO in the modified minimal subtraction ($\overline{\mathrm{MS}}$) factorization scheme by fitting the fractional energy spectra of D_s^+ measured by the OPAL Collaboration in e^-e^+ annihilation on the Z-boson resonance. Authors in Ref. [30] have applied the massless scheme or zero-mass variable-flavor-number scheme (ZM-VFNS) where heavy quarks are treated as any other massless parton. In the present analysis, using the ZM-VFNS we focus on the hadronization of gluon, charm, and bottom quarks into D_s^+ meson and provide the first QCD analysis of $(g, c, b) \to D_s^+$-FFs at next-to-next-to-next-to leading order (NNLO) in perturbative QCD. We also go beyond Ref. [30] by performing a full-fledged error estimation, both for the FFs and the resulting differential cross sections, using the Hessian approach [31]. We will also impose the effect of meson mass on the FFs.

It should be mentioned here that our analysis is restricted to the SIA data only due to the lack of other theoretical partonic cross sections for single inclusive production of partons at NNLO accuracy [32–37]. This allows one to interpret the e^+e^- data of the inclusive single production of hadron at NNLO and thus to extract the corresponding FFs at this order. On the other hand, we are not also aware of any other such data from e^+e^- annihilation; therefore, we are restricted to the SIA data. Although among all processes producing hadrons, the e^+e^- annihilation provides the cleanest laboratory for the extraction of FFs, being devoid of nonperturbative effects beyond fragmentation itself. In the standard model (SM), top quark has a short lifetime so it decays before hadronization takes place. At the lowest order, top quark decays as $t \to bW^+$ followed by $b \to X +$ Jets, where X refers to the detected hadrons in final state. Therefore, at the LHC, the study of energy spectra of produced hadrons through top-quark decays is proposed as a new channel to indirect search for the top-quark properties. As an example of a possible application, the extracted FFs in our phenomenological analysis are used to make the theoretical predictions for the energy distributions of D_s^+ mesons in top decays.

The outline of this paper is as follows: In Sec. II, using the perturbative QCD approach, we provide a general discussion of the fragmentation process for the S-wave heavy meson and determine the fragmentation distribution of c-quark to fragment into D_s^+ meson at LO and NLO. In Sec. III, we describe the theoretical framework of inclusive single hadron production in e^+e^- annihilation through NNLO in the ZM-VFNS and introduce our parametrization of the $c/b \to D_s^+$ FF at the initial scale. In this section, we will also explain the minimization method in our analysis and our approach to error estimation. Our LO, NLO, and NNLO results are presented and compared with the experimental data fitted to. In Sec. IV, we present our NLO predictions for the normalized-energy distributions of D_s^+ mesons from decays of unpolarized top quarks. Our conclusions are presented in Sec. V.

II. THEORETICAL APPROACH TO DETERMINATION OF D_s^+-MESON FFs

Despite that the FFs are related to the low-energy part of hadroproduction processes but, fortunately, it was found that these functions for heavy hadroproductions are analytically calculable by virtue of perturbative QCD (pQCD) with limited phenomenological parameters [16,17]. Historically, the first theoretical attempt to describe the hadroproduction procedure containing heavy quarks was established by Bjorken [38]. In the following, the pQCD approach was applied by Suzuki [26], Ji and Amiri [39] by considering more elaborate models. While in their approach, Suzuki calculates the heavy quark FFs by applying a Feynman diagram similar to that in Figs. 1 and 2, Amiri and Ji calculate their FFs in e^+e^- annihilation process in the same order of pQCD. The Suzuki's model contains most of the kinematical and dynamical properties

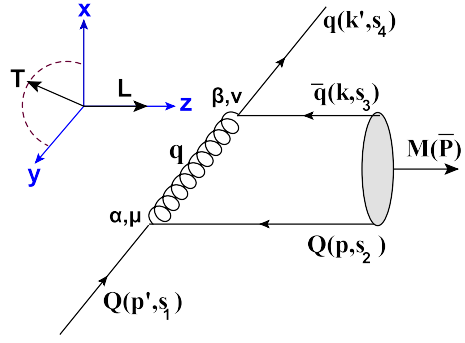

FIG. 1. Lowest-order Feynman diagram contributing to the fragmentation of a heavy quark Q into a heavy meson $M(Q\bar{q})$.

of the fragmentation process and gives one a detailed insight on the hadronization process.

In the following, we briefly describe the Suzuki's model and use it to compute the FF of heavy quark at NLO. According to the Suzuki's model, the FF for the production of an S-wave heavy meson M in the fragmentation of a heavy quark Q may be put in the following form [26]:

$$D_Q^M(z,\mu_0) = \frac{1}{1+2r_i}\sum_{r,c}\int \Pi_f d^3\vec{p}_f |T_M|^2 \delta^3\left(\sum_f \vec{p}_f - \vec{p}_i\right), \tag{1}$$

where μ_0 refers to the initial fragmentation scale, r_i stands for the spin of fragmenting quark, and the summation is going over the spins and colors. In Eq. (1), T_M is the probability amplitude of the meson production which is expressed in terms of the hard scattering amplitude T_H and the process-independent distribution amplitude Φ_M as [39,40]

$$T_M = \int dx_1 dx_2 \delta(1-x_1-x_2) T_H \Phi_M(x_i, Q^2), \tag{2}$$

where x_1 and x_2 are the energy fractions carried by the constituent quarks. This scheme is convenient to absorb the soft behavior of the bound state into the hard scattering amplitude [40]. The short-distance coefficient T_H can be calculated perturbatively from quark-gluon subprocesses at each order of pQCD. The long-distance distribution amplitude Φ_M, which contains the bound state nonperturbative dynamic of the outgoing meson, is the probability amplitude for a quark-antiquark pair to evolve into a particular bound state. The distribution amplitude Φ_M is related to the valence wave function of meson Ψ_M [40]. With the heavy quark mass, the relative motion of the constituent quarks is effectively nonrelativistic and this allows one to estimate the nonrelativistic mesonic wave function as a delta function form. Therefore, the distribution amplitude for an S-wave heavy meson with neglecting the Fermi motion reads [27]

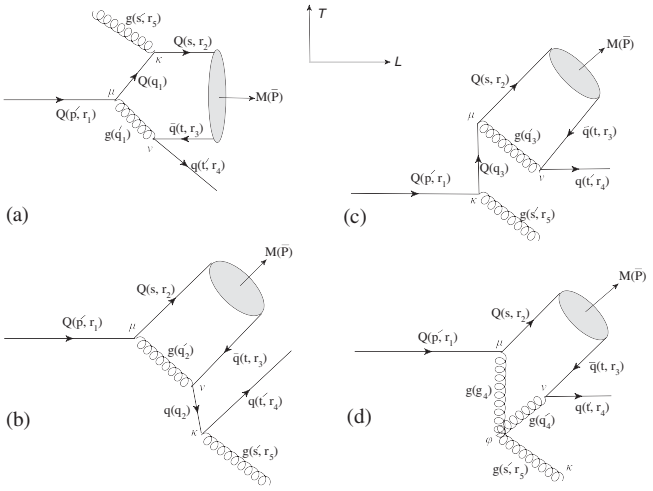

FIG. 2. Production of heavy meson $M(Q\bar{q})$ at NLO pQCD in the Suzuki's model. Real radiative contributions to the process $Q \to M(Q\bar{q}) + q$ are shown at NLO. The spins (r_i) and four-momenta are also labeled.

$$\Phi_M \approx \frac{f_M}{2\sqrt{3}}\delta\left(x_i - \frac{m_i}{M}\right), \tag{3}$$

where $f_M = (6b^3/\pi M)^{1/2}$ refers to the decay constant of meson. With this approximation, we are assuming that the contribution of each constituent quark from the energy of meson (with the mass M) is proportional to its mass, i.e., $x_i = m_i/M$. In Ref. [20], using the Suzuki's model, we derived an analytical expression for the heavy quark FF at lowest order (α_s^2 order) of pQCD by considering the typical Feynman diagram shown in Fig. 1, where a heavy quark Q creates a bound state $M(Q\bar{q})$ along with a light quark q through a single gluon. The result for the fragmentation function $D_{Q\to M}(z,\mu_0)$ depends on the transverse momentum k_T of the initial heavy quark. Here, we present a compacted expression of our previous result, i.e.,

$$\begin{aligned} D_{Q\to M}^{\mathrm{LO}}(z,\mu_0) = {} & \frac{2B^2\alpha_s^2}{3} C_F^2 \frac{z(z-1)^3}{F(z,\langle k_T^2\rangle)} \left\{ \frac{m_Q M^4}{m_q}(1-z)^2 + 2\frac{z(1-z)M^3}{m_q}(m_q m_Q - (1-z)m_Q^2) \right. \\ & + \frac{m_Q M^2}{m_q} z^2((2+3z^2-2z)\langle k_T^2\rangle + 3m_q^2 + 3m_Q^2(1-z)^2 - 8m_q m_Q(1-z)) \\ & \left. - 2\frac{m_Q M}{m_q} z^3([m_Q - (1-z)m_q]\langle k_T^2\rangle + m_q m_Q[m_q - (1-z)m_Q]) + [\langle k_T^2\rangle + m_q^2][\langle k_T^2\rangle + m_Q^2]\frac{m_Q z^4}{m_q} \right\}, \end{aligned} \tag{4}$$

where

$$F(z,\langle k_T^2\rangle) = [(z-1)(M^2 - z m_Q^2) - z(m_q^2 + z\langle k_T^2\rangle)]^2 \times [z^2\langle k_T^2\rangle + (M(z-1) - z m_q)^2]^2 \tag{5}$$

and $B = \pi m_Q m_{\bar{q}} f_M$ but is related to the normalization condition $\int_0^1 D_{Q\to M}(z,\mu_0)dz = 1$ [39].

In computing Eq. (4), following Ref. [26], we adopted the infinite momentum frame where the fragmentation parameter in its usual light-cone form, i.e., $z=(p_M^0+p_M^3)/(p_Q^0+p_Q^3)$, is reduced to a more popular form $z=p_M^0/p_Q^0=E_M/E_Q$, which is more convenient when the masses of partons and outgoing meson are ignored. In reality, the scaling variable z refers to the energy fraction of fragmenting heavy quark which is taken away by the produced meson and takes the values as $0\leq z\leq 1$.

More details on the heavy quark FF at LO, the effects of meson mass, as well as the Fermi motion of constituents can be found in Refs. [20,27].

A. Heavy quark FF at NLO

In this section, we compute an analytical expression for the transverse momentum-dependent FF of heavy quark at NLO ignoring the Fermi motion of constituents. This is done by assumption of a delta function for the meson bound state; see Eq. (3).

Considering the NLO Feynman diagrams shown in Fig. 2, where a produced meson is replaced by its collinear constituents, we make the NLO approximation for the FF of heavy $M(Q\bar{q})$ meson. Considering these Feynman diagrams, we set the relevant four-momenta as

$$\begin{aligned} &p'_\mu=[p'_0,\vec{k}_T,p'_L],\quad s_\mu=[s_0,\vec{0},s_L],\quad s'_\mu=[s'_0,\vec{s'}_T,s'_L]\\ &t'_\mu=[t'_0,\vec{t'}_T,t'_L],\quad t_\mu=[t_0,\vec{0},t_L],\quad \bar{P}_\mu=[\bar{P}_0,\vec{0},\bar{P}_L], \end{aligned} \tag{6}$$

where $\bar{P}$ stands for the four-momentum of the produced meson. Considering the definition of fragmentation parameter, $z=E_M/E_Q=\bar{P}_0/p'_0$, the parton energies can be expressed in terms of the initial heavy quark energy as $s_0=x_1zp'_0, t_0=x_2zp'_0, s'_0\simeq t'_0=(1-z)p'_0/2$, where considering the delta function for meson bound state (3) we are assuming that the contribution of each constituent from the meson energy is proportional to its mass, i.e., $x_1=m_Q/M$ and $x_2=m_{\bar{q}}/M$. Using the kinematics (6), the dot products of relevant four-vectors read

$$\begin{aligned} 2t\cdot t'&=\frac{2m_qz}{M(1-z)}\left(m_q^2+\frac{k_T^2}{4}\right)+\frac{1-z}{2z}m_qM,\\ 2p'\cdot s'&=\frac{k_T^2}{2(1-z)}+\frac{1-z}{2}(m_Q^2+k_T^2)-k_T^2,\\ 2s\cdot p'&=\frac{m_QM}{z}+\frac{zm_Q}{M}(m_Q^2+k_T^2),\\ 2s\cdot s'&=\frac{zm_Q}{2M(1-z)}k_T^2+\frac{1-z}{2z}m_QM. \end{aligned} \tag{7}$$

In Eq. (2), the QCD amplitude T_H is, in essence, the partonic cross section to produce a quark pair $Q\bar{q}$ with certain quantum number that in the old fashioned perturbation theory is expressed as

$$T_H=\frac{g_s^3m_Qm_{\bar{q}}}{2\sqrt{2\bar{P}_0s'_0t'_0p'_0}}C_F\frac{\sum_{i=1}^4\Gamma_i}{\bar{P}_0+s'_0+t'_0-p'_0}, \tag{8}$$

where $C_F=2\sqrt{2}/3$ is the color factor for the process $Q\to M(Q\bar{q})+q+g$, shown in Fig. 2. In Eq. (8), the amplitudes Γ_i stand for each Feynman diagrams in Fig. 2 and include an appropriate combination of the gluon and quark propagators and the spinorial parts of the amplitude. Here, we set the amplitudes Γ_1 for Fig. 2(a), Γ_2 for Fig. 2(b), Γ_3 for Fig. 2(c), and the amplitude Γ_4 for Fig. 2(d). By substituting Eqs. (2), (3), and (8) in Eq. (1) and carrying the necessary integrations out, the heavy quark fragmentation function reads

$$\begin{aligned} D_{Q\to M}^{\text{Real}}(z,\mu_0)=&\frac{A^2\alpha_s^3}{3}C_F^2\int\frac{d^3t'd^3s'}{t'_0s'_0}\int\frac{\sum_{i,j=1}^4\Gamma_i\cdot\Gamma_j^\star}{\bar{P}_0p'_0D_0^2}\\ &\times\delta^3(\vec{\bar{P}}+\vec{t'}+\vec{s'}-\vec{p'})d^3\vec{\bar{P}}, \end{aligned} \tag{9}$$

where $A=\pi^{3/2}f_Mm_qm_Q$ and the factor $D_0=\bar{P}_0+t'_0+s'_0-p'_0$ is the energy denominator. For the phase space integration in the relation (9), one has

$$\int\frac{d^3\vec{\bar{P}}\delta^3(\vec{\bar{P}}+\vec{t'}+\vec{s'}-\vec{p'})}{p'_0\bar{P}_0D_0^2}=\frac{z}{G^2(z)}, \tag{10}$$

where $G(z)=M^2-m_Q^2-m_q^2-2t'\cdot s'+2p'\cdot t'+2p'\cdot s'=M^2+z[zk_T^2+2m_q^2-(1-z)m_Q^2]/(1-z)$. For the remaining integrals, according to the Suzuki's model and for simplicity, we replace the transverse momentum integrations by their average values, e.g.,

$$\int d^3t'\frac{f(z,t'^2_T)}{t'_0}\approx f\left(z,\frac{1}{4}\langle k_T^2\rangle\right), \tag{11}$$

where we assumed $t'_T=k_T/2$ so that $\langle k_T^2\rangle$ is a free parameter which can be specified phenomenologically. Substituting all in Eq. (9), the hadronization process $Q\to M$ is described by the following fragmentation function:

$$D_{Q\to M}^{\text{Real}}(z,\mu_0)=\frac{A^2\alpha_s^3}{3}C_F^2\frac{z}{G^2(z)}\sum_{i,j=1}^4\Gamma_i\cdot\Gamma_j^\star. \tag{12}$$

Using the Dirac algebra and the dot products of four-momenta (7), we simplify the expression $\sum_{i,j=1}^4\Gamma_i\cdot\Gamma_j^\star$. Adopting the Coulomb gauge, it is easy to show that the contribution of fourth Feynman diagram [Fig. 2(d)] to the radiative corrections is zero and other contributions read

$$\sum_{r_i}\Gamma_1\cdot\Gamma_1^\star=\frac{2m_qm_Q}{G_1^2G_2^2}\left\{\frac{m_Q^4}{z^2}(z-1)(19z^2-6z+3)-\frac{m_Q^2k_T^2}{1-z}(21z^2-10z+5)-\frac{z^2k_T^4}{1-z}+\frac{z^4k_T^6}{m_Q^2(1-z)^3}\right\},$$

$$\sum_{r_i}\Gamma_2\cdot\Gamma_2^\star=\frac{24m_q^3}{G_3^2G_4^2}\left\{\frac{m_Q^3}{z^2}(z-1)(3z^2-2z+1)-2\frac{m_Qk_T^2}{1-z}(2z^2-2z+1)-\frac{z^2k_T^4}{m_Q(1-z)}\right\},$$

$$\sum_{r_i}\Gamma_3\cdot\Gamma_3^\star=\frac{2m_q}{G_5^2G_6^2}\left\{\frac{m_Q^5}{z^2}(z-1)(19z^2-6z+3)-\frac{m_Q^3k_T^2}{1-z}(21z^2-10z+5)-\frac{z^2k_T^4}{1-z}m_Q+\frac{z^4k_T^6}{m_Q(1-z)^3}\right\},$$

$$\sum_{r_i}\Gamma_1\cdot\Gamma_2^\star=\frac{-8}{G_1G_2G_3G_4}\frac{m_q}{z^3(1-z)^2m_Q}\times[(1-z)^2m_Q^2+z^2k_T^2]^2\times[z^2k_T^2+m_Q^2(1-2z+3z^2)],$$

$$\sum_{r_i}\Gamma_1\cdot\Gamma_3^\star=\frac{4m_q}{G_1G_2G_5G_6}\left\{\frac{m_Q^5(z-1)}{z^3}(5z^4-2z^3+6z^2-2z+1)-\frac{m_Q^3k_T^2}{z(1-z)}(12z^4-19z^3+21z^2-9z+3)\right.$$
$$\left.-\frac{zm_Qk_T^4}{1-z}(9z^2-6z+3)+\frac{z^3(2z-1)k_T^6}{m_Q(1-z)^2}\right\},$$

$$\sum_{r_i}\Gamma_2\cdot\Gamma_3^\star=\frac{-8}{G_3G_4G_5G_6}\frac{m_q}{z^2(1-z)^2m_Q}\times[z^2k_T^2+m_Q^2(1-2z+3z^2)]\times[z^2k_T^2+(1-z)^2m_Q^2]^2, \tag{13}$$

where the denominators of propagators are expressed as $G_1=2m_q^2+2t\cdot t', G_2=2s\cdot s', G_3=2m_Q^2-2s\cdot p', G_4=2s'\cdot t', G_5=2m_q^2+2t\cdot t'$, and $G_6=-2p'\cdot s'$.

It should be noted that at NLO approximation in addition to the real gluon radiative corrections there are some Feynman diagrams related to the virtual gluon radiative corrections. This new class of diagrams interferes with the LO amplitude, so that the NLO full amplitude is the sum of amplitudes of the Born term (Γ^{LO}), virtual one-loop (Γ^{Loop}), and the real contributions (Γ^{Real}), i.e.,

$$\Gamma^{\mathrm{NLO}}=\Gamma^{\mathrm{LO}}+\Gamma^{\mathrm{Loop}}+\Gamma^{\mathrm{Real}}. \tag{14}$$

The QCD NLO contributions result from the square of these amplitudes, i.e., $|\Gamma^{\mathrm{Born}}|^2=\Gamma^{\mathrm{LO}}\cdot\Gamma^{\mathrm{LO}\star}$ so its related fragmentation function is of order α_s^2; see Eq. (4), $|\Gamma^{\mathrm{Vir}}|^2=2\mathrm{Re}(\Gamma^{\mathrm{LO}}\cdot\Gamma^{\mathrm{Loop}\star})$, and $|\Gamma^{\mathrm{Real}}|^2=\Gamma^{\mathrm{Real}}\cdot\Gamma^{\mathrm{Real}\star}$ so that the NLO fragmentation function is of order α_s^3; see Eq. (12). Note that the Feynman diagrams related to the virtual radiative corrections are classified into two classes. The first class of diagrams includes the fermionic loop diagrams and diagrams with three- and four-gluon vertices. It is shown that these virtual contributions interlock in an essential way. In general, Feynman diagrams with n loops typically contain correction terms proportional to $(\alpha_s\log(Q^2/\Lambda^2))^n$, where Λ is a renormalization scale. Fortunately, these corrections can be absorbed into the lowest-order terms by using the renormalization group equations. In other words, their effect is to modify the gluon propagator by replacing the fixed renormalized coupling with a running coupling constant. Besides these 1PI diagrams, there are also three *tadpole* diagrams, one-loop diagrams with a propagator that connects back to its originating vertex. It is shown that these contributions automatically vanish.

The second class of virtual radiative corrections includes the gluon-quark loops on the incoming or the outgoing quark legs. Generally, these amplitudes need to be considered and included in order to maintain the infrared stability of the overall result. Indeed, these virtual corrections consist of both infrared (IR) and ultraviolet (UV) singularities where the UV divergences appear when the integration region of the internal momentum of the virtual gluon goes to infinity and the IR divergences arise from the soft-gluon singularities. All UV singularities are canceled after summing all virtual contributions up, whereas the IR singularities are remaining. The real gluon radiative corrections also include IR divergences which arise from the soft and collinear gluon emissions. According to the Lee-Nauenberg theorem, after summing, all radiative corrections up the IR singularities cancel each other and the final result is free of all singularities. For more discussion on the IR and UV singularities, see, e.g., Refs. [41–48]. Note that, according to the Suzuki's model, to compute the contribution of real corrections into the fragmentation function we do not integrate over the momentum of the emitted real gluon and instead, we replace the gluon momentum integration by its average value; see Eq. (11). Therefore, by this simplification on the one side, we shall not deal with the IR singularities in the real gluon radiative corrections (12) and on the other side the contribution of the virtual corrections can be ignored. We checked that the contribution of virtual gluon corrections into the QCD amplitude T_H (8) is small and can be ignored.

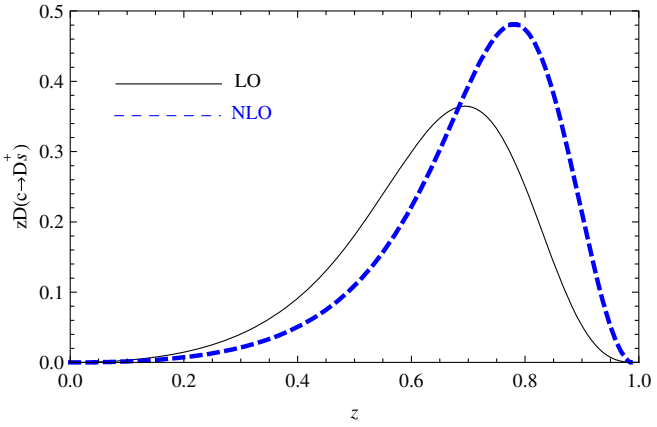

FIG. 3. The FF of $c \to D_s^+$ at LO (solid line) and NLO (dashed line) in the Suzuki's model. The fragmentation scale is $\mu_0 = m_c$ and we set $\langle k_T^2 \rangle = 1$ GeV^2.

Generally, the fragmentation functions depend on both the fragmentation parameter $z = E_M/E_Q (0 \le z \le 1)$ and the fragmentation scale μ. This scale is normally arbitrary, but in a high-energy process of electron-positron annihilation where a jet is produced with transverse momentum k_T, large logarithms of k_T/μ in the partonic cross section of the process $e^+e^- \to Q\bar{Q} \to M(Q\bar{q}) + X$ can be avoided by choosing μ on the order of k_T. Also, the z dependence of the FF is not yet calculable at each desired scale. However, once they are computed at some initial fragmentation scale μ_0, their μ evolution is specified by the DGLAP equations [3]. Therefore, the function (12) should be regarded as a model for the heavy quark FF at the scale μ_0 of order m_Q and the $D_{Q\to M}(z,\mu)$ at larger scales is obtained by solving DGLAP equations.

Here, as an example, we consider the fragmentation of c quark into D_s^+ meson with the constituent quark structure $|D_s^+\rangle = |c\bar{s}\rangle$ taking $f_M = 0.22$ GeV [49] and $\langle k_T^2 \rangle = 1$ GeV^2. In this work, we also consider $\alpha_s(m_c) = 0.38 \pm 0.03$ adjusted such that $\alpha_s(m_Z) = 0.1184$ with $m_Z = 91.18$ GeV. In Fig. 3, the behavior of D_s^+-FF at the initial scale $\mu_0 = m_c$ is shown at the LO (solid line) and NLO (dashed line) QCD approximations. As is seen, higher order QCD corrections shift the peak of fragmentation toward higher-z regions. Except the improvement due to the virtual corrections, we may also think of other effects such as the Fermi motion of constituent quarks and the effects of meson mass, etc.

III. PHENOMENOLOGICAL DETERMINATION OF D_s^+-FFs AND THEIR UNCERTAINTIES

As was explained in the Introduction, more common method to determine the nonperturbative FFs is the phenomenological approach. In this method, the FFs are studying in hadroproduction processes such as electron-positron SIA, lepton-hadron semi-inclusive deep inelastic scattering (SIDIS), and hadron-hadron collisions. Theoretically, the cleanest process to extract the fragmentation densities is SIA because we do not require the simultaneous knowledge of PDFs and FFs. Recently, different analysis have been focused on extracting of FFs for light and heavy hadrons at NLO as well as NNLO accuracies in pQCD [5–10]. The calculation of FFs at high order corrections of pQCD, here we mean NNLO, is possible just for electron-positron annihilation while the calculations for the hard processes in SIDIS and p-p collisions at NNLO are not accessible yet. In this section, we describe the theoretical framework of inclusive single hadron production in e^+e^- annihilation through NNLO in the ZM-FVNS and introduce our parametrizations for the D_s^+-FFs at the initial scale of fragmentation.

A. QCD framework for D_s^+-meson FFs

As was mentioned, in the phenomenological approach, the optimal way to determine the parton FFs is to fit them to all available experimental data. Among all, the best one is the SIA process which occurs via exchange of virtual photon (γ) or Z boson,

$$e^+e^- \to (\gamma^\star, Z) \to D_s^+ + X, \tag{15}$$

where X stands for the unobserved part of final state. Here, our analysis is restricted to the SIA data due to two reasons. First, as explained previously, among all processes producing hadrons the e^+e^- annihilation provides the cleanest environment for the extraction of FFs, being devoid of nonperturbative effects beyond fragmentation itself, i.e., the uncertainties due to PDFs. The second reason is due to the lack of other theoretical partonic cross sections for single inclusive production of partons at NNLO accuracy. This allows us to interpret the e^+e^- data of the inclusive single production of hadron at NNLO and thus to extract the D_s^+-FFs at NNLO. Moreover, we are not aware of any other data for the production of D_s^+ meson.

The partonic cross section of the process (15) is written in terms of three polarized parts [50],

$$\frac{d^2\sigma}{dx_i d\cos\theta} = \frac{3}{8}(1+\cos^2\theta)\frac{d\sigma^T}{dx_i} + \frac{3}{4}\sin^2\theta\frac{d\sigma^L}{dx_i} + \frac{3}{4}\cos\theta\frac{d\sigma^A}{dx_i}, \tag{16}$$

where θ is the scattering angle so this variable is integrated out. The three terms on the right-hand side are related with the transverse, longitudinal, and asymmetric contribution of cross section, respectively. In fact, the first two are associated with the corresponding polarization states of the virtual boson with respect to the direction of the observed hadron and the asymmetric term is due to the parity-violating interference terms and is not present in QED.

These contributions at NLO can be found in Ref. [50] and the extended results up to NNLO are presented in Ref. [37]. Denoting the four-momenta of intermediate gauge boson, produced partons, and hadron by q, p_i, and p_D, respectively, so that $s = q^2$ and $p_D^2 = m_D^2$ we introduce the scaling variables $x_i = 2(p_i \cdot q)/q^2$ and $x_D = 2(p_D \cdot q)/q^2$. Here, $\sqrt{s}$ stands for the collision energy. In the center of mass (CM) frame, the scaling variables are simplified as $x_i = 2E_i/\sqrt{s}$ and $x_D = 2E_D/\sqrt{s}$, where E_i and E_D refer to the energies of partons and D_s^+- meson. In fact, x_i and x_D are the energies of produced partons and meson in units of the beam energy, respectively.

According to the factorization theorem in the QCD-improved parton model [51], the cross section of process (15) can be written as the convolution of differential partonic cross sections $d\sigma_i(e^+e^- \to i + X)/dx_i$ with the $D_i^{D_s^+}$-FFs. In the ZM-VFNS (or zero-mass scheme), where all quarks are treated as massless partons except in the initial conditions of their FFs, one has

$$\frac{d\sigma}{dx_D}(e^+e^- \to D_s^+ + X) = \sum_i \int_{x_D}^1 \frac{dx_i}{x_i} \frac{d\sigma_i}{dx_i}(x_i, \mu_R, \mu_F) D_i^{D_s^+}\left(\frac{x_D}{x_i}, \mu_F\right), \quad (17)$$

where $i = g, u, \bar{u}, \ldots, b, \bar{b}$ runs over the active partons. Here, μ_R and μ_F are the renormalization and factorization scales, respectively, which are *a priori* arbitrary but a typical choice is $\mu_R = \mu_F = \sqrt{s}$ [52] to avoid the logarithmic term $\ln(s/\mu_F^2)$ appearing in differential partonic cross sections. In Eq. (17), the differential hard-scattering cross sections $d\sigma_i/dx_i$ are known up to NNLO in perturbative QCD [32–37] and the $D_i^{D_s^+}(z, \mu_F)$-FF describes the nonperturbative part of the process (15) related to the transition $i \to D_s^+$. In the CM frame, the fragmentation parameter $z = x_D/x_i$ is the fraction of energy passed on from parton i to the charmed meson, like the definition in Sec. II. It is customary in experimental analyses to normalize Eq. (17) by the total hadronic cross section,

$$\sigma_{\rm tot} = \frac{4\pi\alpha^2(s)}{s}\left(\sum_i^{n_f} \tilde{e}_i^2(s)\right)(1 + \alpha_s K_{\rm QCD}^{(1)} + \alpha_s^2 K_{\rm QCD}^{(2)} + \cdots), \quad (18)$$

where $\tilde{e}_i$ is the effective electroweak charge of quark i, α and α_s are the fine-structure and strong-coupling constants, respectively, and the coefficient $K_{\rm QCD}^{(n)}$ contains the N^{n}LO correction. Here, we need $K_{\rm QCD}^{(1)} = 3C_F/(4\pi)$ and $K_{\rm QCD}^{(2)} \approx 1.411$ [53].

It should be noted that the factorization formula presented in Eq. (17) is proved provided that the mass of quarks and hadron is ignored. In Ref. [7], we have proved how to enter the hadron mass effects into the inclusive hadron production in e^+e^- reaction. To incorporate the hadron mass effects, we used a specific choice of scaling variables by working in the light-cone coordinates. Ignoring the detail of calculations, as a generalization of the massless case, the factorization relation in the presence of hadron mass m_H reads

$$\frac{d\sigma}{dx_H}(x_H, s) = \frac{1}{1 - \frac{m_H^2}{s\eta^2(x_H)}} \frac{d\sigma}{d\eta}(\eta(x_H), s), \quad (19)$$

where $\eta = x_H/2 \times (1 - 4m_H^2/(sx_H^2))$ and

$$\frac{d\sigma}{d\eta}(\eta, s) = \sum_i \int_\eta^1 \frac{dy}{y} \frac{d\hat{\sigma}_i}{dy} D_i^H\left(\frac{\eta}{y}, \mu_F\right). \quad (20)$$

The above relation will be a basic formula for the factorization theorem extended in the presence of hadron mass and would be more effective and applicable when the data are presented in lower energy scales. As a considerable point, the effect of hadron mass is to increases the cross section $d\sigma/dx_H$ at small x_H so this treatment acts inverse for large x_H. We incorporated the mass corrections into the publicly available `APFEL` package [54] which is used to determine the free parameters of FFs.

The z distribution of the $(c, b) \to D_s^+$-FFs at the starting scale μ_0 is a genuinely nonperturbative quantity to be extracted from experimental data. Their forms are unknown, and an educated guess is in order. The selection criterion is to score a minimum χ^2 value as small as possible with a set of fit parameters as minimal as possible. Due to few numbers of experimental data for D_s^+-meson production, it is not possible to constrain b and c quarks in the same parametrization form; thus, following Ref. [30], we adopt two different parametrization forms for the $c \to D_s^+$ and $b \to D_s^+$ FFs. Since the charm distribution usually dominates at large z, we use the optimal functional form for the parametrization of charm suggested by Peterson *et al.* [55] as

$$D_c^{D_s^+}(z, \mu_0^2) = N_c \frac{z(1-z)^2}{[(1-z)^2 + \epsilon z]^2}, \quad (21)$$

which includes two free parameters N_c and ϵ. For the $b \to D_s^+$ transition, we use the following simple power form [30]:

$$D_b^{D_s^+}(z, \mu_0^2) = N_b z^\alpha (1-z)^\beta, \quad (22)$$

including three unknown and free parameters N_b, α, and β. These forms were found to enable excellent fits. The free parameters will be extracted from a global fit on experimental data measured by OPAL Collaboration [28,29] at the CERN LEP1 collider. In this analysis, the FFs are

parametrized at the initial scale $\mu_0^2 = 18.5\ \mathrm{GeV}^2$, which is a little grater than the b-quark mass threshold, and then evolved to the scale of experimental measurements. At the initial scale μ_0, the FFs of light quarks and gluon are assumed to be zero so that they will be generated through DGLAP equations [3] to higher values of μ_F.

In our analysis, we employ the publicly available APFEL package [54] in order to the evolution of $zD^{D_s^+}(z,\mu^2)$-FFs as well as for the calculation of SIA cross sections up to NNLO accuracy. The free parameters of FFs are determined by minimizing the $\chi^2_{\texttt{global}}$ function using the CERN program MINUIT [56]. This function is defined in our previous work in detail [9]. This quantity includes the overall normalization errors of the D-meson productions datasets. Note also that, to estimate the FFs uncertainties, the experimental data uncertainties are propagated to the extracted QCD fit parameters using the asymmetric Hessian method, as outlined in [57,58]. In this method, a confidence region is identified by providing the tolerance criterion $\Delta\chi^2$. There is no unique criterion for selecting the correct value of $\Delta\chi^2$ in the various global analysis. In some analysis, the value of $\Delta\chi^2 = 1$ has been chosen as a standard tolerance criterion [59]. To be more precise, in such analysis, the $\Delta\chi^2$ value is calculated such that the confidence level P becomes the one σ error range ($P = 0.6826$) for only one parameter. In fact, the main argument for such choice is that for the Gaussian distributions the parameter errors in χ^2 fits should be determined by $\Delta\chi^2 = 1$ irrespective of the number of free parameters in the fit [60]. This approach is usually called Hessian methodology.

B. Experimental data and fit result

Defining our framework, we are now in a situation to perform our analysis of D_s^+-FFs using available SIA experimental data. For input parameters, we set the charm- and bottom-quark masses as $m_c = 1.67$ GeV and $m_b = 4.3$ GeV, respectively, and take the strong coupling $\alpha_s^{(n_f)}$ in the $\overline{\mathrm{MS}}$ scheme with $n_f = 5$ active quark flavors adjusted such that $\alpha_s^{(n_f)}(M_Z) = 0.1184$ for $M_Z = 91.2$ GeV [49]. For the charm fragmentation into D_s^+ meson via SIA process, there are the B-factory CLEO [61] and Z-factory OPAL [28] datasets. The CLEO Collaboration released their its results for $\sigma(D_s)$ at energies near to the $\Upsilon(4S)$ resonance 10.5 GeV. Moreover, CLEO Collaboration has presented its results for the scaled momentum spectra $d\sigma/dx_p$, where the scaled momentum fraction is defined as $x_p \equiv |\vec{p}|/|\vec{p}_{\max}|$ with

$$p_{\max}(D_s) = \sqrt{E_{\mathrm{beam}}^2 - m_{D_s}^2}, \tag{23}$$

where E_{beam} and m_{D_s} stand for the beam energy and the mass of D_s meson, respectively. Since the CLEO and the OPAL Collaborations reported their results for $d\sigma/x_p$ and $d\sigma/x_D$, respectively, then one needs a relation between the scaled momentum and energy fractions, i.e., x_p and x_D. This is achieved by the following relation [50]:

$$x_p = \sqrt{\frac{x_D^2 - \rho_H}{1 - \rho_H}}, \tag{24}$$

where $\rho_H = 4m_H^2/s$. For differential cross section, the conversion formula is [50]

$$\frac{d\sigma(x_p)}{dx_p} = (1 - \rho_H)\frac{x_p}{x_D}\frac{d\sigma(x_D)}{dx_D}. \tag{25}$$

Since the variable x_D ranges as $\sqrt{\rho_H} \le x_D \le 1$, then x_p ranges from $x_p = 0$ to $x_p = 1$. The APLFEL code [54], used in our analysis, is set for $1/\sigma_{\texttt{tot}} \times d\sigma/dx_D$, so using the equation above we rescaled the CLEO dataset in this form and included into our analysis. Although the CLEO data can provide useful information on the D_s^+-FFs, but there is a problem in using them in our analysis. In fact, on the one hand, we are employing the ZM-VFNS in our analysis, which is reliable only for high-energy scales, while the data from CLEO are located much close to the thresholds $\sqrt{s} = 2m_c$ and $\sqrt{s} = 2m_b$ of the transitions $c \to H_c$ and $b \to H_b$. The OPAL results have been reported at the Z-boson resonance, i.e., $\sqrt{s} = 91.2$ GeV, which is much higher than the CLEO one for which $\sqrt{s} = 10.5$ GeV. On the other hand, the CLEO Collaboration has not included the corrections due to electromagnetic initial-state radiation in the SIA process [50,62]. Consequently, we realized that the inclusion of CLEO dataset leads to a tension and increases the value of χ^2/d.o.f. Therefore, we excluded the CLEO data and restricted ourselves to the OPAL dataset [28]. In the SIA process, two mechanisms contribute with similar rate; $Z \to c\bar{c}$ decay followed by $c/\bar{c} \to D_s^+$ fragmentation and $Z \to b\bar{b}$ decay followed by $b/\bar{b} \to H_b$ fragmentation and weak decay of the bottom-flavored hadron H_b into the charmed meson via $H_b \to D_s^+ + X$. Note that the energy spectrum of D_s^+ meson originating from decays of H_b hadrons is much softer than that due to primary charm production. For separating charmed hadron production through $Z \to c\bar{c}$ decay from $Z \to b\bar{b}$ decay, OPAL used the apparent decay length distributions and energy spectra of the charmed hadrons. The decay lengths of H_b hadrons into H_c ones are longer than those from prompt production.

OPAL Collaboration has presented x_D distributions for D_s^+ sample and for the $z \to b\bar{b}$ subsamples (b-tagged events). The datasets are displayed in the form $1/N_{\mathrm{had}} \times dN/dx_D$, where N is the number of charmed meson candidates reconstructed through appropriate decay chains. To convert these data into the desired cross section $1/\sigma_{\texttt{tot}} \times d\sigma/dx_D$, one should divide them by the

TABLE I. The individual χ^2 values for inclusive and b-tagged cross sections obtained by OPAL Collaboration [28] at LO, NLO, and NNLO. The total χ^2 and χ^2/d.o.f. fit for D_s^+ is also shown.

Data properties	$\sqrt{s}$ GeV	Data points	χ^2 (LO)	χ^2 (NLO)	χ^2 (NNLO)
Inclusive	91.2	8	0.037	0.025	0.022
b tagged	91.2	8	0.123	0.103	0.098
Total		16	0.160	0.128	0.121
(χ^2/d.o.f.)			0.082	0.064	0.060

convenient branching fractions of decays used in Refs. [28,29] for the reconstruction of charmed mesons, i.e.,

$$\mathrm{Br}(D_s \to \phi\pi^+) = (3.5 \pm 0.4)\%. \tag{26}$$

The characteristics of available experimental data along with the values of χ^2 are presented in Table I. We also presented the total χ^2 divided by the number of degrees of freedom at LO (χ^2/d.o.f. = 0.082), NLO (χ^2/d.o.f. = 0.064), and NNLO (χ^2/d.o.f. = 0.060). These values show a well-satisfying fit. As expected on general grounds, χ^2/d.o.f. is reduced as one passes from LO to NNLO. These results are extracted including the hadron mass effect. Our analysis shows that the inclusion of meson mass leads to a reduction in the value of $\chi^2/(\mathrm{d.o.f.})$ up to about 4%. However, due to the scale of energy given for the data used in our work, i.e., $\sqrt{s} = 91.2$ GeV, this improvement is small but having the data at lower energies, it is expected to have more effect on the $\chi^2/(\mathrm{d.o.f.})$.

After introducing the experimental data used in our analysis, we now present our results obtained through the QCD fit. The optimal values of the free parameters expressed in the models considered for the FFs, Eqs. (21) and (22), at the initial scale $\mu_0^2 = 18.5$ GeV^2 are listed in Table II at the LO, NLO, and NNLO accuracies. In Fig. 4, we plotted the z distributions of the LO, NLO, and NNLO D_s^+-FFs with their uncertainties at higher energy scale $\mu = 10$ GeV. To this aim, we studied the $(c, b, g) \to D_s^+$-FF at LO (solid lines), NLO (dashed lines), and NNLO (dot-dashed lines). As is seen, the charm-quark fragmentation is peaked at large z, whereas the one due to bottom-quark fragmentation has its maximum at small z. This is due to the fact that the fragmentation process $b \to D_s^+$ contains two-step mechanism including $b \to X_b$ fragmentation followed by the weak $X_b \to D_s^+ + X$ decay of the bottom-flavored hadron X_b. Figure 4 does also include the $g \to D_s^+$-FF, which is generated via DGLAP evolution from the initial condition $D_g^{D_s^+}(z, \mu_0) = 0$, as was explained previously.

TABLE II. The optimal values for the fit parameters in Eqs. (21) and (22) at the initial scale $\mu_0^2 = 18.5$ GeV^2 determined by QCD analysis of the experimental data listed in Table I.

Parameter	Best values LO	NLO	NNLO
N_c	0.176	0.176	0.176
ϵ	0.108	0.141	0.155
N_b	1.555	1.359	1.380
α	0.318	0.206	0.203
β	1.859	1.923	1.983

In Fig. 4, the KK06 results [30] (dot-dashed-dashed lines) are also shown for comparison. In Ref. [30], the starting scales for the charm and bottom FFs are taken to be $\mu_0 = m_c = 1.5$ GeV and $\mu_0 = m_b = 5$ GeV, respectively. As is seen from Fig. 4, our results for the bottom and gluon fragmentations are in good agreement with the ones presented by KK06. In comparison to the KK06's results, there is a considerable difference between the KK06 charm FF and ours over the whole range of z. A reason for this inconsistency might be due to the different initial energy scales chosen. In Fig. 5, our LO, NLO, and NNLO theoretical predictions for SIA cross sections evaluated with our respective D_s^+-meson FF sets are shown at the scale $\mu = 91.2$ GeV and are compared with the experimental data fitted to, so as to check directly the consistency and goodness of our fits. As is seen, our results are in a good agreement with OPAL datasets particularly for b-tagged ones. It is also seen that higher order corrections can make a better consistency between the theoretical predictions and the experimental data. Although other improvements such as those from inclusion of heavy quarks masses can make better consistencies. These effects are considered in the general-mass variable-flavor-number scheme (GM-VFNS) [50]. In Fig. 5, we have also shown the uncertainty bands which are needed to visually quantify the remaining error of our analysis.

In this work, we extracted the FF of $c \to D_s^+$ through two different approaches. To check the validity of our theoretical model, i.e., the Suzuki's model, using the parameters presented in Table II we plotted the $D_c^{D_s^+}(z, \mu_0)$-FF in Fig. 6 at different accuracies, i.e., LO (solid line), NLO (dashed line), and NNLO (dot-dashed line). The LO, NLO, and NNLO results agree in the shape and the position of maximum, but differ in normalization. This difference is induced by higher order radiative corrections $\mathcal{O}(\alpha_s^2)$ in the hard-scattering cross sections and in the timelike splitting functions, and it is compensated in the physical cross sections to be compared with the experimental data up to terms beyond $\mathcal{O}(\alpha_s^2)$. In Fig. 6, we have also plotted the $D_c^{D_s^+}(z, \mu_0)$-FF at NLO QCD approximation obtained through the Suzuki's model (dotted line); see also Fig. 3. A considerable agreement between both approaches can be seen which ensures the validity of the Suzuki's model.

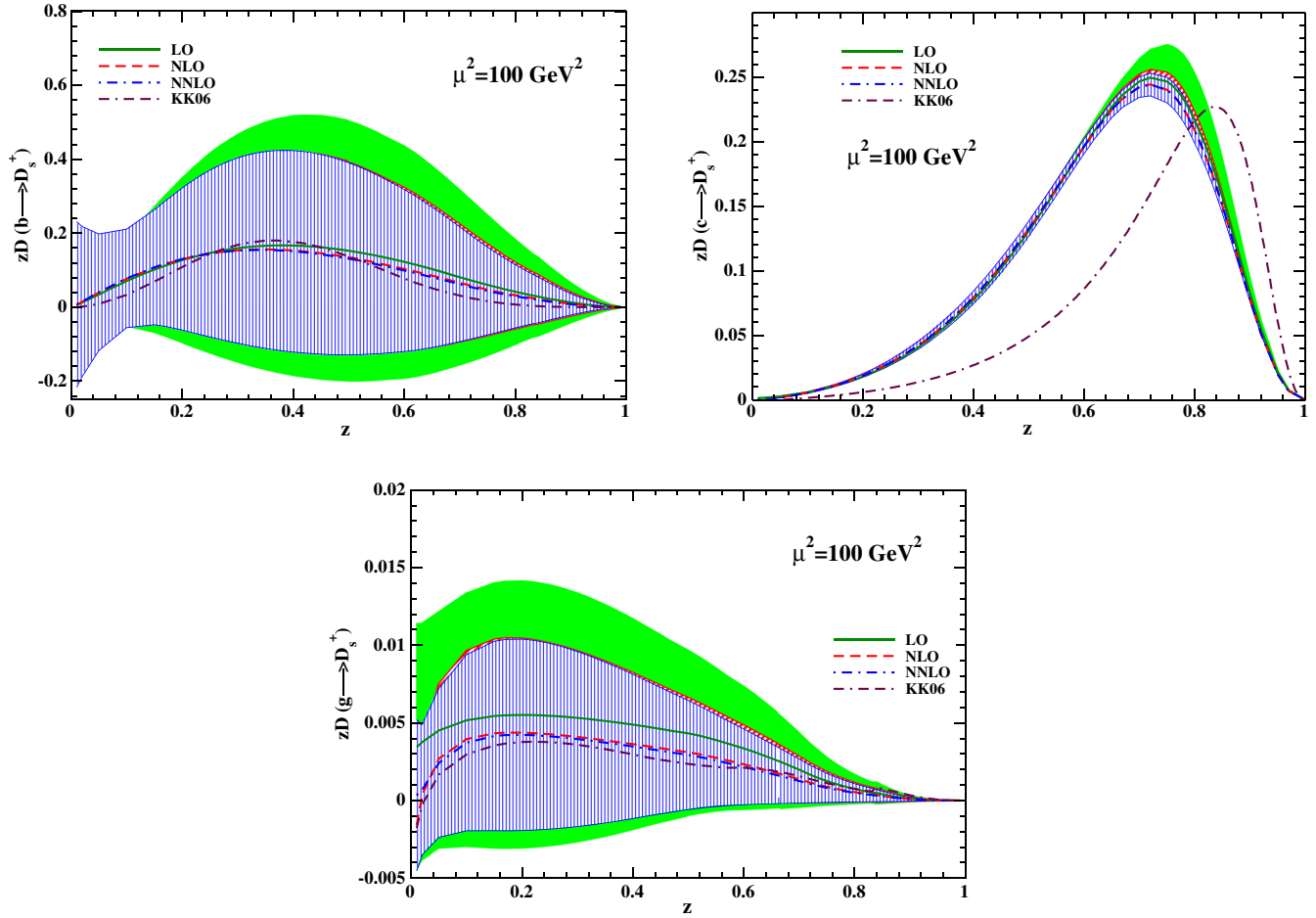

FIG. 4. The bottom-, charm-, and gluon-FFs with their uncertainties obtained at LO (solid lines), NLO (dashed lines), and NNLO (dot-dashed lines) QCD analyses of D_s^+-meson productions. The KK06 results [30] (dot-dashed-dashed lines) are shown for comparison.

IV. CHARMED MESON PRODUCTION BY TOP-QUARK DECAY

Charmed mesons may be produced directly or through the decay of heavier particles, including the Z boson, the Higgs boson, and the top quark. At the LHC, the study of energy spectrum of produced mesons through top decays might be considered as an indirect channel to search for the top-quark properties. As a topical application of

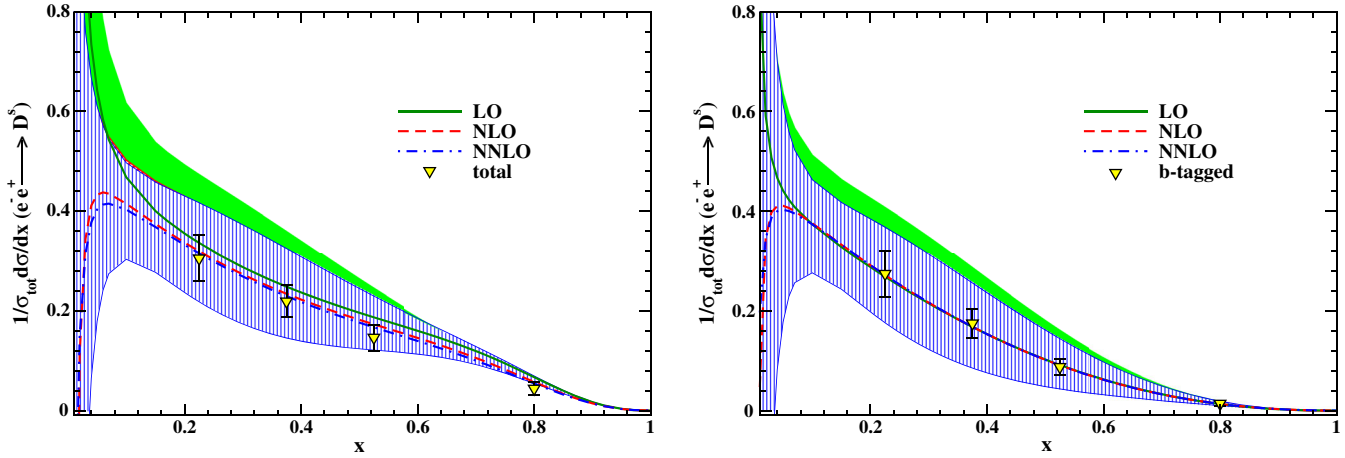

FIG. 5. Our LO, NLO and NNLO theoretical predictions are compared with the normalized inclusive total (right) and b-tagged (left) data sets for D_s^+ meson production from OPAL experiment. Corresponding uncertainty bands are also shown.

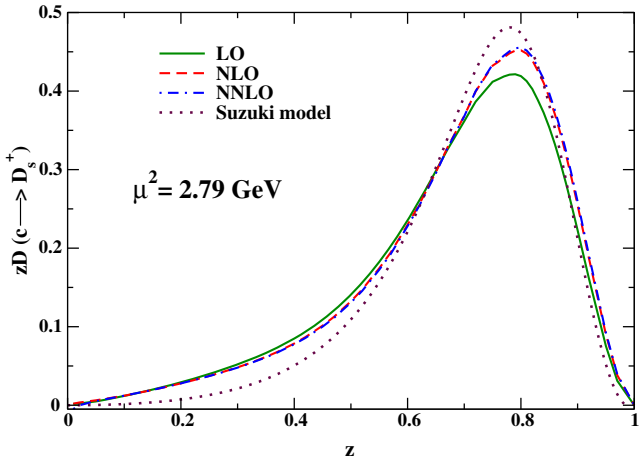

FIG. 6. The $c \to D_s^+$ FF at LO (solid line), NLO (dashed line), and NNLO (dot-dashed line) extracted through the phenomenological approach at the initial scale μ_0. These are compared with the one extracted through the Suzuki's model (dotted line) at NLO; see Fig. 3.

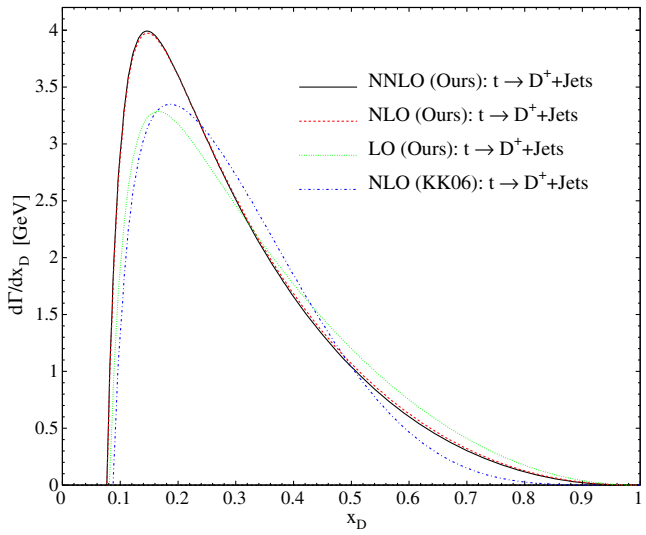

FIG. 7. $d\Gamma(t \to D_s^+ + \text{Jets})/dx_D$ as a function of x_D at LO (dots), NLO (dashed line), and NNLO (solid line) accuracies at $\mu = m_t$. Our results are also compared with the NLO one from KK06 [30] (dot-dashed).

our analysis, here we study inclusive single D_s^+-meson production through the following process:

$$t \to b + W^+(g) \to W^+ + D_s^+ + X, \tag{27}$$

where X collectively denotes any other final-state particles. At the parton level in the process (27), both the b-quark and gluon may hadronize into the charmed mesons. Gluon fragmentation contributes to the real radiations at NLO and higher orders. The partial width of the process (27) differential in the scaled D_s^+ energy, x_D, in the ZM-VFNS reads

$$\frac{d\Gamma}{dx_D} = \sum_{i=b,g} \int_{x_i^{\min}}^{x_i^{\max}} \frac{dx_i}{x_i} \frac{d\Gamma_i}{dx_i}(\mu_R, \mu_F) D_i^{D_s^+}\left(\frac{x_D}{x_i}, \mu_F\right), \tag{28}$$

where in the top-quark rest frame, we have $x_D = E_D/E_b^{\max}$ and $x_i = E_i/E_b^{\max}$, where E_D and E_i are the energies of the D_s^+ hadron and parton i, and $E_b^{\max}$ is the maximum energy of the bottom quark. In our application of the ZM-VFNS, where $m_b \ll \mu_F = \mathcal{O}(m_t)$, the bottom quark is taken to be massless. By the same token, we also neglect the charmed meson mass m_D. So far, $d\Gamma_i/dx_i$ are only available through NLO; analytic expressions may be found in [63,64]. Although a consistent analysis is presently limited to NLO, we also employ our NNLO D_s^+-meson FF set to explore the possible size of the NNLO corrections.

In (28), the factorization (μ_F) and the renormalization (μ_R) scales are arbitrary but to remove the large logarithms which appear in the differential decay rate, here, we set them to $\mu_R = \mu_F = m_t$.

Adopting $m_W = 80.379$ GeV and $m_t = 173.0$ GeV, in Fig. 7, we plotted the energy distribution of D_s^+ meson produced in the unpolarized top-quark decay at LO (dots), NLO (dashed line), and NNLO (solid line) accuracies at $\mu = m_t$. It is observed that switching from the LO D_s^+-meson FF set to the NLO one leads to enhancement in the theoretical prediction in the peak region and reduction it in the tail region thereunder. At the same time, the peak position is shifted toward smaller values of x_D. Results at NNLO are the same as in NLO accuracy; however, for the NNLO spectrum, we are using the partonic differential decay rates $d\Gamma_i/dx_i$ which are only available up to NLO. These effects should mark an lower limit of the total NNLO corrections because the as-yet-unknown NNLO corrections to $d\Gamma_i/dx_i$ are expected to give rise to some compensation if FF universality is realized in nature. Using the NLO FFs of $(b, g) \to D_s^+$ from Ref. [30], we have also compared our results with the one from the KK06 Collaboration (dot-dashed). As is seen, in comparison with the KK06 result, our FFs lead to an enhancement in the energy spectrum of D_s^+ meson at the peak position.

At the CERN LHC, the study of the energy spectrum of charmed mesons can be also considered as a new window toward searches on new physics. In other words, any considerable deviation of energy distribution of mesons from the SM theoretical predictions can be related to the new physics [65,66].

V. SUMMARY AND CONCLUSIONS

In this paper, we determined the nonperturbative FFs for the charmed meson D_s^+ in two various methods: theoretical and phenomenological approaches, and compared them. In the theoretical approach, we computed the D_s^+-FF both at LO and NLO using the Suzuki's model in the QCD framework. In the phenomenological approach,

we determined the D_s^+-FFs both at LO, NLO and, for the first time, at NNLO in the ZM-VFNS, by fitting to all available experimental data of inclusive single D_s^+-meson production in e^+e^- annihilation, $e^+e^- \to D_s^+ + X$, from OPAL Collaboration [29]. The theoretical framework provided by the zero-mass scheme was quite appropriate for the present analysis, since the characteristic energy scales of the considered process, M_Z, greatly exceeded the charm- and bottom-quark masses, which could thus be neglected. In our analysis, we have adopted the optimal functional form for the parametrization of charm FF suggested by Peterson et al., Eq. (21), with two free parameters and the simple power ansatz of Eq. (22) for the $b \to D_s^+$ transition with three free parameters. Then, we obtained for the fit parameters appearing therein the values listed in Table II. For the lowest-order approximation, as is seen in Fig. 5, the behavior of cross section given theoretically is not acceptable at low-x region so it goes to infinity when $x \to 0$. This treats reasonably when the NLO and NNLO radiative corrections are imposed. Moreover, the goodness of the LO, NLO, and NNLO fits turned out to be excellent, with χ^2/d.o.f. values of 0.082, 0.064, and 0.060, respectively (see Table I). As expected on general grounds, the fit quality is improved by ascending to higher orders of perturbation theory. Our analysis improves a similar one in the literature [30] in the following respects. For the first time, we advanced to NNLO in a fit of D_s^+-meson FFs; however, this correction is tiny. We performed an estimation of the experimental uncertainties in our D_s^+-hadron FFs using the Hessian approach. We have also imposed the effect of meson mass on the corresponding FFs. On the other side, we have compared, for the first time, the analytical results obtained through the Suzuki's model with the ones extracted through the phenomenological approach. We found good consistency between both approaches; see Fig. 6.

As a typical application of extracted FFs, we employed the LO, NLO, and NNLO FFs to make theoretical predictions for the scaled-energy distributions of D_s^+ meson inclusively produced in top-quark decays. We encourage the LHC Collaboration to measure the x_D distribution of the partial width of the decay $t \to D_s^+ W^+ + X$, for two reasons. On the one hand, this will allow for an independent determination of the D_s^+-hadron FFs and thus provide a unique chance to test their universality and DGLAP scaling violations, two important pillars of the QCD-improved parton model of QCD. On the other hand, this provides a new window toward searches on new physics.

Possible theoretical improvements via the phenomenological approach include the inclusion of finite quark masses and the resummation of soft-gluon logarithms, which extend the validity toward small values of x_D, and the resummation of threshold logarithms, which extends the validity toward large values of x_D. The general-mass variable-flavor-number scheme [42] provides a consistent and natural finite mass generalization of the ZM-VFNS on the basis of the $\overline{\text{MS}}$ factorization scheme [51]. Possible improvements via the theoretical approach include the inclusion of Fermi motion of constituents by considering the real aspects of the valence wave function of meson Ψ_M [40], etc.

[1] A. P. Martynenko and V. A. Saleev, Phys. Rev. D **53**, 6666 (1996).
[2] E. Braaten and T. C. Yuan, Phys. Rev. Lett. **71**, 1673 (1993).
[3] V. N. Gribov and L. N. Lipatov, Yad. Fiz. **15**, 781 (1972) [Sov. J. Nucl. Phys. **15**, 438 (1972)]; G. Altarelli and G. Parisi, Nucl. Phys. **B126**, 298 (1977).
[4] B. A. Kniehl, G. Kramer, I. Schienbein, and H. Spiesberger, Eur. Phys. J. C **72**, 2082 (2012).
[5] J. Binnewies, B. A. Kniehl, and G. Kramer, Phys. Rev. D **58**, 034016 (1998).
[6] B. A. Kniehl, G. Kramer, I. Schienbein, and H. Spiesberger, Phys. Rev. D **77**, 014011 (2008).
[7] S. M. M. Nejad, M. Soleymaninia, and A. Maktoubian, Eur. Phys. J. A **52**, 316 (2016).
[8] M. Soleymaninia, H. Khanpour, and S. M. M. Nejad, Phys. Rev. D **97**, 074014 (2018).
[9] M. Salajegheh, S. M. M. Nejad, H. Khanpour, B. A. Kniehl, and M. Soleymaninia, Phys. Rev. D **99**, 114001 (2019).
[10] M. Salajegheh, S. M. M. Nejad, M. Soleymaninia, H. Khanpour, and S. A. Tehrani, arXiv:1904.09832.
[11] M. Soleymaninia, M. Goharipour, and H. Khanpour, Phys. Rev. D **98**, 074002 (2018).
[12] M. Soleymaninia, M. Goharipour, and H. Khanpour, Phys. Rev. D **99**, 034024 (2019).
[13] A. Mohamaditabar, F. Taghavi-Shahri, H. Khanpour, and M. Soleymaninia, Eur. Phys. J. A **55**, 185 (2019).
[14] D. P. Anderle, F. Ringer, and M. Stratmann, Phys. Rev. D **92**, 114017 (2015).
[15] V. Bertone, S. Carrazza, N. P. Hartland, E. R. Nocera, and J. Rojo (NNPDF Collaboration), Eur. Phys. J. C **77**, 516 (2017).
[16] J. P. Ma, Nucl. Phys. **B506**, 329 (1997).
[17] E. Braaten, K. M. Cheung, and T. C. Yuan, Phys. Rev. D **48**, 4230 (1993).
[18] S. M. M. Nejad, Phys. Rev. D **96**, 114021 (2017).
[19] M. Delpasand and S. M. M. Nejad, Phys. Rev. D **99**, 114028 (2019).
[20] S. M. M. Nejad and A. Armat, Eur. Phys. J. Plus **128**, 121 (2013).
[21] S. M. M. Nejad and E. Tajik, Eur. Phys. J. A **54**, 174 (2018).

[22] S. M. M. Nejad and A. Armat, Eur. Phys. J. A **54**, 118 (2018).
[23] S. M. M. Nejad and P. S. Yarahmadi, Eur. Phys. J. A **52**, 315 (2016).
[24] S. M M. Nejad and D. Mahdi, Int. J. Mod. Phys. A **30**, 1550179 (2015).
[25] S. M. M. Nejad, Eur. Phys. J. Plus **130**, 136 (2015).
[26] M. Suzuki, Phys. Lett. B **71**, 139 (1977).
[27] S. M. M. Nejad, Eur. Phys. J. A **52**, 127 (2016).
[28] G. Alexander *et al.* (OPAL Collaboration), Z. Phys. C **72**, 1 (1996).
[29] K. Ackerstaff *et al.* (OPAL Collaboration), Eur. Phys. J. C **1**, 439 (1998).
[30] B. A. Kniehl and G. Kramer, Phys. Rev. D **74**, 037502 (2006).
[31] J. Pumplin, D. R. Stump, and W. K. Tung, Phys. Rev. D **65**, 014011 (2001).
[32] A. Mitov, S. Moch, and A. Vogt, Phys. Lett. B **638**, 61 (2006).
[33] A. A. Almasy, S. Moch, and A. Vogt, Nucl. Phys. **B854**, 133 (2012).
[34] P. J. Rijken and W. L. van Neerven, Phys. Lett. B **386**, 422 (1996).
[35] P. J. Rijken and W. L. van Neerven, Phys. Lett. B **392**, 207 (1997).
[36] P. J. Rijken and W. L. van Neerven, Nucl. Phys. **B487**, 233 (1997).
[37] A. Mitov and S. O. Moch, Nucl. Phys. **B751**, 18 (2006).
[38] J. D. Bjorken, Phys. Rev. D **17**, 171 (1978).
[39] F. Amiri and C.-R. Ji, Phys. Lett. B **195**, 593 (1987).
[40] S. J. Brodsky and C. R. Ji, Phys. Rev. Lett. **55**, 2257 (1985).
[41] S. M. M. Nejad, Eur. Phys. J. C **72**, 2224 (2012).
[42] S. M. M. Nejad and M. Balali, Eur. Phys. J. C **76**, 173 (2016).
[43] S. M. M. Nejad, Nucl. Phys. **B905**, 217 (2016).
[44] S. M. M. Nejad and M. Balali, Phys. Rev. D **90**, 114017 (2014).
[45] S. M. M. Nejad, S. Abbaspour, and R. Farashahian, Phys. Rev. D **99**, 095012 (2019).
[46] S. Abbaspour, S. M. M. Nejad, and M. Balali, Nucl. Phys. **B932**, 505 (2018).
[47] S. Abbaspour and S. M. M. Nejad, Nucl. Phys. **B930**, 270 (2018).
[48] S. M. M. Nejad, Phys. Rev. D **85**, 054010 (2012).
[49] M. Tanabashi *et al.* (Particle Data Group), Phys. Rev. D **98**, 030001 (2018).
[50] T. Kneesch, B. A. Kniehl, G. Kramer, and I. Schienbein, Nucl. Phys. **B799**, 34 (2008).
[51] J. C. Collins, Phys. Rev. D **58**, 094002 (1998).
[52] D. P. Anderle, T. Kaufmann, M. Stratmann, F. Ringer, and I. Vitev, Phys. Rev. D **96**, 034028 (2017).
[53] K. G. Chetyrkin, A. L. Kataev, and F. V. Tkachov, Phys. Lett. **85B**, 277 (1979).
[54] V. Bertone, S. Carrazza, and J. Rojo, Comput. Phys. Commun. **185**, 1647 (2014).
[55] C. Peterson, D. Schlatter, I. Schmitt, and P. M. Zerwas, Phys. Rev. D **27**, 105 (1983).
[56] F. James and M. Roos, Comput. Phys. Commun. **10**, 343 (1975).
[57] A. D. Martin, W. J. Stirling, R. S. Thorne, and G. Watt, Eur. Phys. J. C **63**, 189 (2009).
[58] D. Stump, J. Pumplin, R. Brock, D. Casey, J. Huston, J. Kalk, H. L. Lai, and W. K. Tung, Phys. Rev. D **65**, 014012 (2001).
[59] S. Alekhin, J. Blümlein, S. Moch, and R. Placakyte, Phys. Rev. D **96**, 014011 (2017).
[60] G. Aad *et al.* (ATLAS Collaboration), Eur. Phys. J. C **73**, 2509 (2013).
[61] R. A. Briere *et al.* (CLEO Collaboration), Phys. Rev. D **62**, 072003 (2000).
[62] M. Cacciari, P. Nason, and C. Oleari, J. High Energy Phys. 04 (2006) 006.
[63] S. M. M. Nejad, Phys. Rev. D **88**, 094011 (2013).
[64] B. A. Kniehl, G. Kramer, and S. M. M. Nejad, Nucl. Phys. **B862**, 720 (2012).
[65] S. M. M. Nejad and S. Abbaspour, Nucl. Phys. **B921**, 86 (2017).
[66] S. M. M. Nejad and S. Abbaspour, J. High Energy Phys. 03 (2017) 051.